# Passive coherent multistatic SAR using spaceborne illuminators

Nithirochananont, Ussanai; Antoniou, Michail; Cherniakov, Mike

*DOI:*
10.1049/iet-rsn.2019.0425



*Document Version*
Peer reviewed version

*Citation for published version (Harvard):*
Nithirochananont, U, Antoniou, M & Cherniakov, M 2020, 'Passive coherent multistatic SAR using spaceborne illuminators', *IET Radar, Sonar and Navigation*. https://doi.org/10.1049/iet-rsn.2019.0425

# Passive coherent multistatic SAR using spaceborne illuminators

Ussanai Nithirochananont, Michail Antoniou *, and Mikhail Cherniakov

[1] Department of Electronic, Electrical and Systems Engineering, University of Birmingham, Edgbaston B15 2TT, Birmingham, United Kingdom
*m.antoniou@bham.ac.uk

**Abstract: This paper shows methodology of experimentation and experimental results on coherent passive multistatic Synthetic Aperture Radar (SAR) using Global Navigation Satellite Systems (GNSS) as transmitters of opportunity. An experimental campaign at the proof of concept level was conducted using transmission from two satellite apertures and a fixed receiver, to emulate a coherent multistatic SAR acquisition. The acquired signals from a point-like source as well as an extended target area were analysed in terms of their K-space support, and then coherently combined to improve spatial resolution. The obtained multistatic results from both experiments confirm that a coherent combination of SAR images with such a system is possible and improves the overall system performance.**

## 1. Introduction

A passive SAR system uses transmitters of opportunity to form radar imagery. In this configuration, the non-cooperative source is typically a satellite or a terrestrial transmitter, and motion of either or both the transmitter and the receiver are used to form a synthetic aperture. A variety of transmitting sources and receiver configurations have so far been used to obtain a number of experimental radar images [1-6]. In this paper we concentrate on passive SAR where the transmitter is a moving satellite and the receiver is fixed on the ground (Fig. 1). An example of such a satellite transmitter is GNSS (e.g. GPS or Galileo), which has been considered for a number of years on the theoretical and experimental levels [7-15].

Regardless of the illuminating platform, a general limitation of passive SAR is the spatial resolution it can achieve, and GNSS-based SAR is no exception. This is because resolution is directly dependent on the transmit waveform bandwidth, which is not only beyond user control but was also not originally designed for radar applications. For example, the maximum bandwidth of a single GNSS ranging signal is approximately 10 MHz (e.g. Galileo E5a/b or GPS L5), which allows a quasi-monostatic range resolution of 15 m. Therefore, in recent years, a number of efforts have been dedicated to improve it. In one such work, it was shown possible to combine the Galileo E5 bands to an aggregate bandwidth of 50 MHz, but at the cost of SAR sensitivity, which is an issue in GNSS-based SAR due to the low power flux density of GNSS, and near the ground [16].

Another option is to improve spatial resolution by combining SAR images obtained by spatially separated transmitters. This is particularly promising for spaceborne illuminators, including GNSS, since numerous spaceborne systems comprise constellations of satellites for global and persistent services. GNSS-based SAR in particular is inherently a multistatic system. Given a single GNSS constellation, 6-8 satellites can simultaneously illuminate any point on Earth, from different viewing angles, with highly stable clocks that may potentially be considered as coherent over a reasonable time. A single receiver can receive and separate these transmitted signals due to their multiple access scheme, which can then be used to form independent bistatic images that can subsequently be combined, either coherently or non-coherently [17]. In terms of non-coherent combination, it was shown that two satellites can provide a substantial improvement in resolution, but to do so requires special satellite trajectories and complex signal processing to compensate for artefacts arising from non-coherent techniques [18-19].

The natural next step is to attempt spatial resolution improvement using a coherent combination of multiple passive bistatic SAR images obtained from satellite transmitters at slightly different viewing angles. The general theory for coherent multistatic SAR using multiple monostatic platforms is well-known and has been proven over numerous publications, e.g. [20-23], but for bistatic and especially passive configurations results are more limited and usually confined to confirmations using simulated data, at least in the open literature [24-30]. In [24], coherent combination technique was shown under laboratory conditions that can provide substantial improvement over its bistatic counterparts. A number of works with various multistatic configurations, in terms of number of platforms, have been contributed at simulation level. Their results show promising, similar effects [25-30].

The goal of this paper is to understand the feasibility of passive coherent multistatic SAR with GNSS illuminators of opportunity and experimentally assess it. This is done firstly by investigating k-space support in passive multistastic SAR with spaceborne illuminators, and applying it to the GNSS-based SAR case. The emphasis of the paper is on the experimental confirmation of this concept, which is based on an experimental proof-of-concept campaign both with a point-like target and with an extended target area. By verifying this concept, spatial resolution improvement for GNSS-based SAR is confirmed, and the experimental platform developed can be used to understand general aspects of coherent multistatic SAR more deeply.

The paper is organised as follows: Section 2 briefly provides a basis for coherent image combination in our system. Section 3 describes the experimental campaign. Section 4 presents and discusses results of coherent

multistatic SAR obtained from a point-like target and a real target area, and Section 5 concludes the paper.

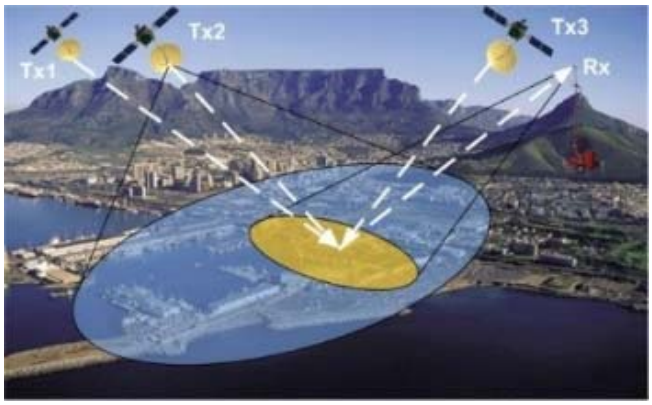


**Fig. 1 The concept of passive GNSS-based SAR with a fixed receiver on the ground**

## 2. K-space support and coherent combination

Coherent combination for multistatic SAR generally requires both coherent scattering and signal coherence between transmitters and receivers. For the former case, this translates to strict conditions on the spatial separation between the transmit/receive platforms. This is a major limiting factor in the passive multistatic SAR with spaceborne illuminators since satellite trajectories cannot be controlled for this purpose. In this paper it is assumed that coherent scattering conditions are met. It is beyond its scope of this paper to investigate when the coherent scattering conditions break, since this is a complex problem that needs a dedicated study of its own. However, the coherent scattering assumption can fundamentally be made. This is due to the high number of satellites illuminating a point on Earth, both simultaneously (6-8 satellites for each GNSS constellation, for example, while numerous constellations now share the same frequency bands e.g. Galileo E5a and GPS L5) and within short temporal intervals.

For the latter case, signal coherence in multistatic SAR can be maintained even if transmitters or receivers have independent clocks, in a similar manner to how bistatic systems deal with this problem. Considering a constellation of transmit satellites and a single receiver on the ground, the receiver records all satellite signal reflections and all direct satellite signals through the same receiving channels, which have common clocks. Therefore, all receiver artefacts are common to all satellite signals, while relative clock drift between the different transmit sources can be compensated differentially by using direct satellite signals as the reference signals for matched filtering with target echoes. This concept has been proposed, e.g. [30], with high possibility of having signal coherence using one satellite with an on-board transmitter and multiple receive-only satellites follow the transmitting satellite on the same orbit.

Having established coherent scattering and signal coherence, multistatic SAR image combination can be viewed by determining the k-space support of individual bistatic images. The location, shape and extent of the SAR data in this domain are determined by the transmitting carrier frequency and bandwidth, as well as the relative geometries of the different platforms. If two or more bistatic SAR datasets have overlapping or adjacent k-space supports, then they can be coherently added to create a single SAR data set. This set has a wider k-space extent, which in turn implies a refined spatial resolution, possibly both in range and cross-range.

### 2.1. Monostatic configuration

In a monostatic configuration, where the transmitter and receiver are co-located (i.e. zero angular separation), SAR echoes can be represented in the spatial frequency domain as fractions of the wavenumber, $k = 2\pi f_c/c$, where $f_c$ is the carrier frequency and $c$ is speed of light. If a target is assumed at the origin and a platform were to move over an azimuth span of 360˚, signal samples would trace a circular k-space support whose centre point is at origin and radius is $2k$ (Fig. 2 (a)), taking into account round-trip propagation. From [31], its components in the $k_x$ (range) and $k_y$ (cross-range) directions are expressed as

$$k_x = 2kcos(\theta), \tag{1}$$

$$k_y = 2ksin(\theta). \tag{2}$$

### 2.2. Bistatic configuration

In the general bistatic case, the angular separation between platforms should considered and the radar signal travels in the direction of the bisector of the bistatic angle. Therefore, after transforming from a polar format derived in [32] into a Cartesian grid, the location of a signal sample in the spatial frequency domain depends on the transmitter and receiver locations and is expressed as

$$2kcos(\tfrac{\theta_T-\theta_R}{2}) = (4\pi f_c/c)cos(\tfrac{\theta_T-\theta_R}{2}), \tag{3}$$

where $\theta_T$ is the azimuth angle of the transmitter, $\theta_R$ is the azimuth angle of the receiver and $(\theta_T - \theta_R)$ is the bistatic angle. In this case, each component in the $k_x$ and $k_y$ axes is given by

$$\begin{aligned} k_x &= 2kcos\left(\tfrac{\theta_T-\theta_R}{2}\right)cos\left(\tfrac{\theta_T+\theta_R}{2}\right) \\ &= k(cos\theta_T + cos\theta_R), \end{aligned} \tag{4}$$

$$\begin{aligned} k_y &= 2kcos\left(\tfrac{\theta_T-\theta_R}{2}\right)sin\left(\tfrac{\theta_T+\theta_R}{2}\right) \\ &= k(sin\theta_T + sin\theta_R). \end{aligned} \tag{5}$$

The k-space support for the general bistatic configuration is shown in Fig. 2 (b) where a solid red circle represents a case when transmitter moves over 360˚ of azimuth plane with one fixed receiver position. When a receiver moves to another fixed position, signal samples will be formed as a new circle (dashed red circle). This means a centre point of a circle in the bistatic configuration depends on both a transmitter and a receiver positions. Comparing k-space from the monostatic and the general bistatic cases (Fig. 2), k-space support is changed from a circle whose centre point is at origin to a circle whose circumference pass the origin.

In the bistatic case with a fixed receiver, as in GNSS-based SAR, the receiver can be assumed to be at 0˚, similar to [33], and Eq. (4)-(5) then become

$$k_x = k(cos\theta_T + 1), \tag{6}$$

$$k_y = ksin\theta_T, \tag{7}$$

and the k-space support will be a solid-line circle in Fig. 2(b).

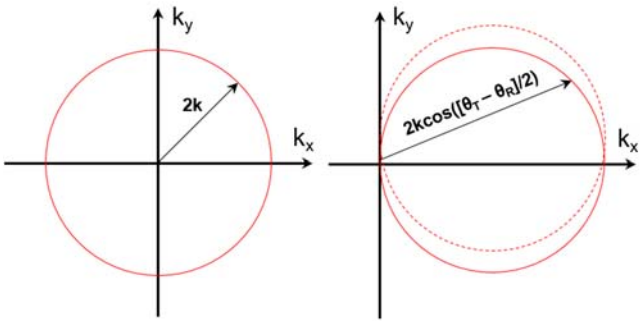


(a) (b)

**Fig. 2 K-space support for (a) monostatic and (b) general bistatic configurations**

### 2.3. Coherent multistatic GNSS-based SAR

The multistatic configuration can be considered as a combination of multiple bistatic pairs. A multistatic configuration of passive SAR with spaceborne illuminators and a fixed receiver, such as GNSS-based SAR, can employ $M$ satellites and a fixed receiver. Each $m^{th}$ satellite moves along a trajectory with an azimuth angle of $\theta_{Tm}$ whereas angular position of the fixed receiver, $\theta_R$, is defined at 0° relative to the x-axis (Fig. 3). Each satellite uses a ranging code with bandwidth $B$. For any given target, the components of the k-space support for each transmitter - receiver pair are determined, based on [34] and (6)-(7), by

$$k_x = \frac{2\pi(f_c+f_b)}{c} \times \left(cos\left(\theta_{Tm,k}\right) + 1\right), \quad (8)$$

$$k_y = \frac{2\pi(f_c+f_b)}{c} \times sin\left(\theta_{Tm,k}\right), \quad (9)$$

where $\theta_{Tm,k}$ is the $k^{th}$ azimuth position of the $m^{th}$ satellite, and $f_b$ is the $b^{th}$ frequency within the bandwidth of the ranging code. In this case, assuming $B$ and the transmitter's azimuth span are sufficiently narrow, the k-space support takes an approximately rectangular shape.

An example k-space support for this case is shown in Fig. 4, using two spatially separated satellites that transmit in the same carrier frequency. Despite the platforms are at different positions, their k-space supports are laid on the same circle as they employ the same carrier frequency and the same fixed receiver.

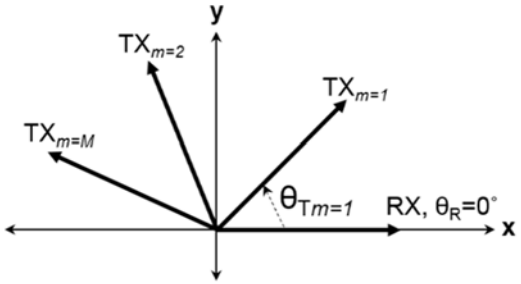


**Fig. 3 Multistatic GNSS-based SAR imaging geometry**

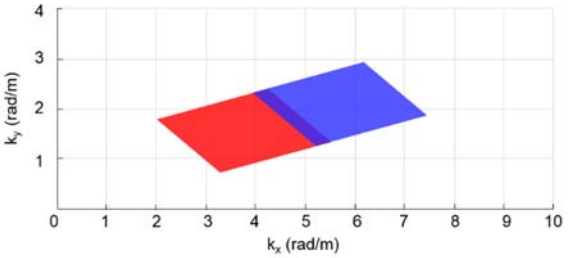


**Fig. 4 Example of multistatic GNSS-based SAR k-space support**

If two or more data acquisitions have adjacent k-space supports based on Eq. (8)-(9), and the other limitations described at the start of the section are met, the appropriate received signals can be coherently combined. In such case, a coherent multistatic image can be formed by summing complex value of the corresponding bistatic images of those appropriate signals on a pixel-by-pixel basis using

$$I_M = \frac{1}{N}\left|\sum_{i=1}^{N} I_i\right|, \quad (10)$$

where $I_M$ is the multistatic image, $I_i$ is the $i^{th}$ bistatic image and $N$ is a total number of bistatic images used in the combination. Combining images in this manner creates a single multistatic image with an extended k-space support that is the superposition of those manifested by the individual bistatic images used in the combination, which results in an enhanced spatial resolution.

## 3. Experimental campaign

### 3.1. Experiment design

The purpose of the experimental campaign was to experimentally validate the possibility of coherently combining passive SAR images with multiple spaceborne illuminators and a fixed receiver to enable a spatial resolution improvement. GNSS were used in the campaign as transmitters of opportunity. The validation was split in two steps. In the first step, a single point-like target was used, and in the second, an extended target area.

In order to obtain proof of concept and compare experimental results to theoretical expectations, a simplified multistatic configuration was used, which emulated two spatially separated transmitters and a single fixed receiver on the ground. The two separated transmitters were emulated by taking two temporally separated datasets from the same GNSS satellite, during its pass over the target area. The two apertures were temporally separated, instead of simply splitting a single aperture in two halves, in order for a more representative multistatic scenario to be considered.

### 3.2. The experimental system

The experimental system was installed at the roof of the Gisbert Kapp building, at the University of Birmingham, approximately 35 m above the ground. The experimental system consists of a GNSS receiver and two antennas (Fig. 5). The receiver was the SX-3, a software-defined radio originally built by IFEN GmbH for navigation purposes and converted into a GNSS-based SAR through a European Space Agency (ESA) grant. Its performance has been demonstrated with a single transmitter and a single receiver in [35].

The receiver has two channels, one recording direct satellite signals (Heterodyne Channel, HC) for signal synchronisation, and another one collecting reflected signals

off the target area (Radar Channel, RC) for imaging. The HC had a low-gain (6 dB) antenna pointed towards the sky, while the RC had a high-gain antenna (15 dB) pointed towards the target area.

**Fig. 5 Experimental testbed**

### *3.3. Bistatic image formation*

Bistatic image formation for GNSS-based SAR is well documented [9], [15], so only a short overview is presented here. A block diagram of the signal processing required for image formation is shown in Fig. 6. The first step is to perform signal synchronisation on the HC data, to maintain signal coherence needed for image formation. This is done by tracking the direct signal from each satellite in the field of view of the HC antenna, in a manner similar to that used in navigation. At the output of this step, a replica of the direct signal is constructed using the tracked direct signal parameters and the GNSS ranging code, which can then be used as the reference signal for the range compression step of the image formation algorithm. In practice, the synchronisation is implemented by the SX3 in near real-time. Subsequently, the range-compressed data are processed into passive SAR imagery using a Back-Projection Algorithm (BPA), which incorporates positional information for each transmitter as well as the receiver.

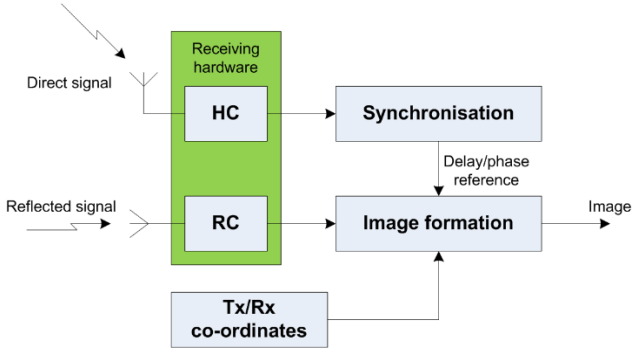


**Fig. 6 Block diagram of bistatic GNSS-based SAR image formation**

### *3.4. Point-like target and extended target area*

A point-like target was used in the first validation step. In bistatic SAR systems, using calibrated targets such as corner reflectors is not recommended since their radar cross section (RCS) is less predictable [36], a problem that is especially acute for passive SAR such as the one used in this research where the power flux density near the ground is relatively low . As another option, the HC antenna can serve as a point-like target at zero range from the receiver [13]. In this scheme, the direct signal can be processed using the BPA into a corresponding point spread function (PSF) of the point-like target (HC antenna).

In the second validation step, an extended target area was used. This was part of the University of Birmingham campus and was located to the west of our receiver location. The area approximates an urban setting on the left-hand side and a rural environment on the other side (Fig. 7). The urban area is dense with complex buildings whereas two large sport pitches and tree lines are the main distinct features on the right-hand side. Distinctive features in the target area include sports fields, residence towers (~1.2 km range) marked as target (A), tree lines (at ~850 m range) marked as target (B), as well as Women's Hospital (C) at ~900 m range.


**Fig. 7 Target area**

### *3.5. Data collection*

To obtain the required data described above, k-space support was used to predict datasets to be acquired. As mentioned in Section 3.1, in order to compare experimental results with well-known theoretical expectations, two separated transmitters were emulated by taking two temporally separated datasets from the same satellite, GPS BIIF-05-30, during one of its passes above the target area. Its L5 signal was recorded for 10 minutes in each dataset, with a 5-minute gap between acquisitions. In this way, the two datasets may be viewed as sub-apertures, and coherent multistatic results can be compared to bistatic results that would be expected had the full aperture been used instead, because in the latter case we can use previously derived, accurate analytical descriptions of the PSF [15] for comparison.

K-space support extents for the two datasets were determined using Eq. (8)-(9). The experimental parameters used in the calculation are shown in Table 1. Figure 8 shows

the obtained k-space support extents from the two datasets. A small gap (~0.2 rad/m in both $k_x$ and $k_y$) between the two k-spaces can be noticed, resulting from the temporal separation between datasets. This gap was sufficiently small to maintain the coherence and verify coherent combination results against those of a single aperture without the intermediate gap, at the expense of higher sidelobes in multistatic results. The total k-space support is extended in both directions compared to the individual k-space supports, and therefore we can expect an improved spatial resolution in both range and azimuth. It is noted that the gap in Fig. 8 may visually similar to loss data in interrupted SAR (IntSAR) [37], but the multistatic results shown later that the gap was not exhibited as missing data in the resultant PSF or image as in the case of interrupted SAR.

**Table 1 Parameters of the experiment**

| Parameters | Value |
|---|---|
| Satellite | GPS BIIF-05-30 |
| Carrier Frequency | 1176.45 MHz |
| Ranging code bandwidth | 10.23 MHz |
| Dwell time on target | 10 min (with 5 min gap) |
| Acquisition 1 Azimuth | 171.622˚-172.647˚ |
| Acquisition 1 Elevation | 34.340˚-39.056˚ |
| Acquisition 2 Azimuth | 169.668˚-171.166˚ |
| Acquisition 2 Elevation | 41.432˚-46.205˚ |

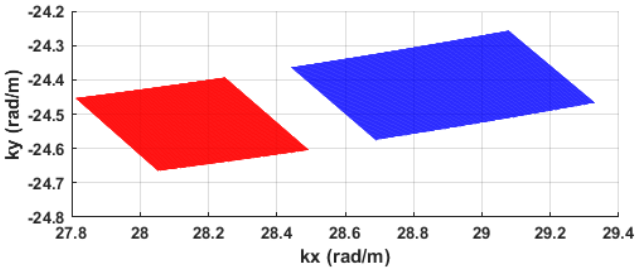


**Fig. 8 K-space support obtained from the two datasets**

## 4. Experimental results

### *4.1. Point-like target results*

The combination technique was validated using the point-like target by obtaining their corresponding experimental PSFs. Fig. 9 (a)-(b) shows the experimental bistatic PSFs (BPSF 1 and 2, obtained from the first and second acquisitions, respectively) of the target [38]. Both PSFs are similar in orientation since the positions of the satellite were only slightly different. As a result, both PSFs also have similar spatial resolutions, shown in Table 2, which are 3-4 m in cross-range and 17-19 m in range.

Fig. 9 (c) shows the experimental coherent multistatic PSF (MPSF) obtained by coherently combining the aforementioned bistatic PSFs [38]. This was compared to the theoretical PSF that would be obtained if a bistatic image formation was performed on the full aperture rather than the two sub-apertures used (i.e. from the start of acquisition 1 until the end of acquisition 2, without a gap between them), using [11] (Fig. 9 (d)). Therefore, if the coherent combination was successful, Figs. 9 (c) and (d) should be the same. Overall, both are in good agreement which verifies the multistatic methodology used.

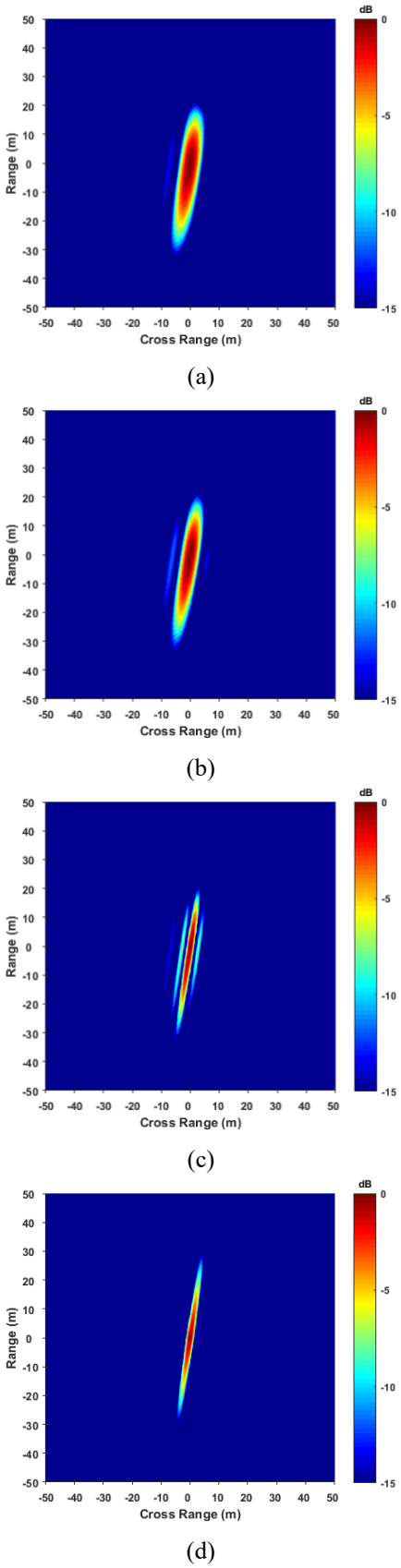


**Fig. 9 Experimental PSFs (a) BPSF 1, (b) BPSF 2, (c) experimental coherent MPSF, (d) theoretically expected BPSF for full aperture**

Comparing the coherent MPSF to the two BPSF [38], it can be seen that the multistatic PSF is much narrower than the individual bistatic PSFs. Cross-sectional plots in cross-range and range (Fig. 10) show a comparison between these PSFs, where red, black, and blue lines represent BPSF 1, BPSF 2, and coherent MPSF, respectively. The narrower mainlobe is prominent with the blue lines. This confirms improvement in spatial resolution, with quantitative results shown in Table 2. The improvement in both directions is a consequence of extending the total k-space support (Fig. 8) in both $k_x$and $k_y$. Another observation is that the improvement in the multistatic case is approximately doubling the bistatic counterparts and consistent with size of the total k-space extent relative to individual extents, as expected.

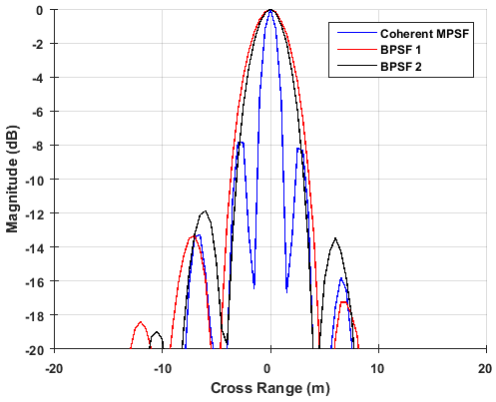


(a)

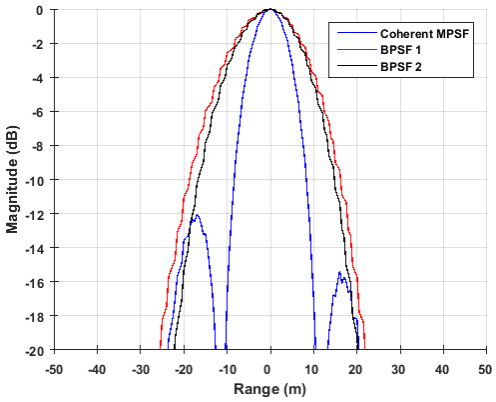


(b)

**Fig. 10 Comparison between the experimental coherent MPSF and the individual BPSFs in (a) Cross-range and (b) Range**

**Table 2 Spatial resolution comparison of experimental PSFs**

| PSF | Cross-range (m) | Range (m) |
|---|---|---|
| BPSF 1 | 4.281 | 19.343 |
| BPSF 2 | 3.656 | 17.406 |
| Coherent MPSF | 1.437 | 9.875 |

In addition, slightly high sidelobes can be seen in the resultant coherent multistatic PSF in Fig. 9 (c) compared to the theoretical PSF in Fig. 9 (d) and this is expected due to a small gap in the experimental data. In this case, the sidelobe level of the experiment coherent MPSF (Fig. 11) is below -7 dB in the cross-range and below -12 dB in the range which is still deemed practical. As a result, this confirms that, at the system level, coherent combination using the system is possible and enable finer spatial resolution.

It is noted that the results were presented in their original form to show maximum resolution performance of the coherent multistatic technique. In our particular case, the gap between data collections is narrow enough to apply sidelobe reduction techniques, including windowing and nonlinear weighting, which can suppress this high sidelobe level with different expenses. For example, a Kaiser window was applied to the experimental multistatic PSF (Fig. 9 (c)). As a result, the sidelobe level was reduced to approximately -12 dB (Fig. 12). In cases where the spectral gap is wider, however, these methods are unlikely to be effective and the development or application of suitable spectral estimation techniques (e.g. [39]-[40]) might be more appropriate, but this research is beyond the scope of this paper. In the next section, validation was done using the same method and was applied to the real target area to evaluate whether an improvement is still valid at image level.

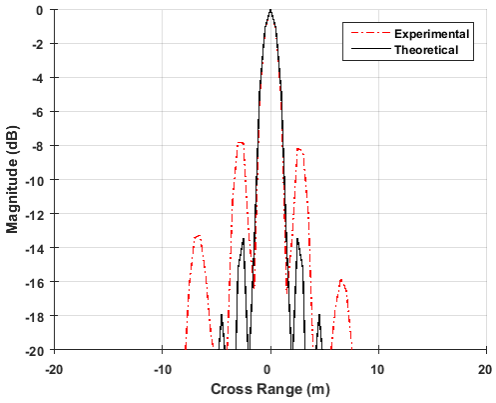


(a)

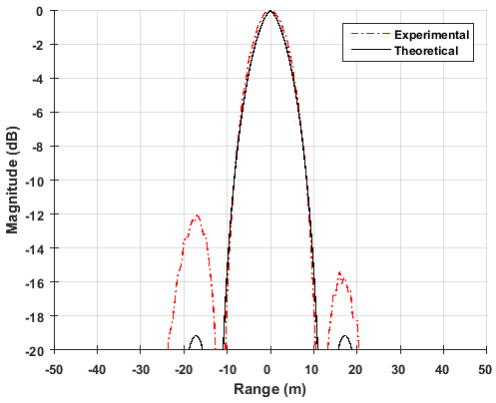


(b)

**Fig. 11 Comparison between the experimental and theoretically expected coherent multistatic PSFs in (a) Cross-range and (b) Range**

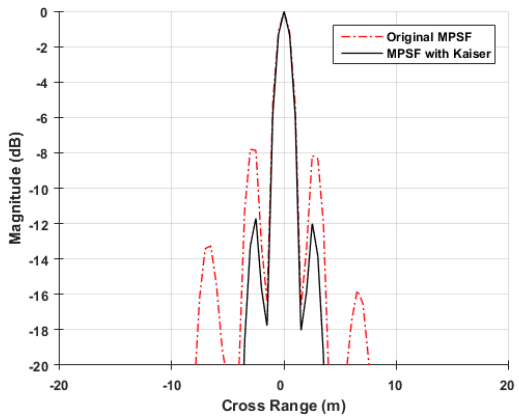


**Fig. 12 Comparison between the experimental coherent MPSF before and after applying Kaiser window in Cross-range**

### *4.2. Target area results*

The dataset captured from the radar channel of the receiver were used to produce the bistatic images of the target area. These datasets contain signals reflected off the real target area in Fig. 7. They were then processed into bistatic images using the same algorithms as in the case of the point-like target datasets. Fig. 13 (a)-(b) shows the obtained experimental bistatic images.

Visually, the appearance of echoes in both images are in a similar pattern which is due to similarity of their imaging geometries, as was the case with the point-like target. The tree lines in the middle of the scene (between 50-200 m cross-range) are prominent in both images. The diagonal line emanating from 100 m cross-range and spanning the length of the image is an artefact of the direct signal present in the radar data. This direct signal, which is received through the sidelobes of the RC antenna, and its multipath versions comprise interference that limit the sensitivity and dynamic range of the system [41-42], however as the goal here is to assess spatial resolution improvement, direct path interference effects can be neglected by examining areas in the image that do not exhibit it. In more general terms, methods for its removal are possible (e.g. [43]-[44]), but their evaluation and/or modification for this system is a separate research study beyond the scope of the paper. In passing, it is also noted that multi-path clutter is not visible in Fig. 13, which has been observed in imagery from earlier publications (e.g. [7]-[12]) and is accredited to the relatively low sensitivity of the system [15].

These bistatic images were then formed a multistatic image using coherent combination. Fig. 13 (c) shows the obtained coherent multistatic image. Comparing bistatic and multistatic results, it is seen that there are additional compressed echoes in the coherent multistatic image which are also narrower than those in the bistatic images. Both of these effects are indicators of improved resolution. Examples of this improvement from the three parts across the images (the area A-C) are shown in Fig. 14, 16 and 18. This improvement also conforms to those in the point-like target case.

To further investigate, the compressed echoes from the images were analysed in terms of their spatial resolution. In this case, a distinct compressed echo in each enlargement image was selected (marked by red arrow). Their cross-sectional profiles in both range and cross-range are shown in Fig. 15, 17 and 19. Their -3 dB resolutions were measured and are listed in Tables 3-5. The results show that spatial resolutions from all target areas were improved in the coherent multistatic image. It is also seen that the spatial resolution of the experimental PSFs from the images are similar to those from the point-like target (i.e. system PSF).

In terms of echo intensity, the coherent multistatic results have approximately 6 dB improvement over the bistatic counterparts (see Fig. 15, 17 and 19). This is theoretically expected as two images with the same dwell time on target are being coherently summed. Both the spatial resolution and echo intensity improvements verify the validity of passive coherent multistatic SAR with spaceborne illuminators, and the approach followed here to achieve it.

## 5. Conclusions and future work

This paper presents methods of introducing coherent multistatic SAR capability for passive systems with spaceborne illuminators and a fixed receiver, with the goal of spatial resolution improvement. The proposed methodology requires deriving the k-space support for bistatic SAR images obtained from this kind of system of individual bistatic images, before coherently combining them. To understand the validity of the model, and the ultimate feasibility of such a system, an experimental system was built, and an experimental campaign was conducted with both point-like targets and extended target areas. The illuminators of opportunity used for experimentation were GNSS, however the approach followed here is agnostic of the illumination type and therefore can be applied to other satellite systems. The results show that the system is feasible, and it can be realised with the proposed method.

Future work will concentrate on expanding the proposed concept to numerous satellites in order to expand the k-space support, and hence spatial resolution, even further. To achieve that, research will be needed in two parallel directions. The first one will require the study of relative transmitter orientations needed to provide contiguous k-space support and coherent target scattering, while the second one will investigate methods of filling spectral gaps between such acquisitions for the general case where k-space continuity cannot be guaranteed.

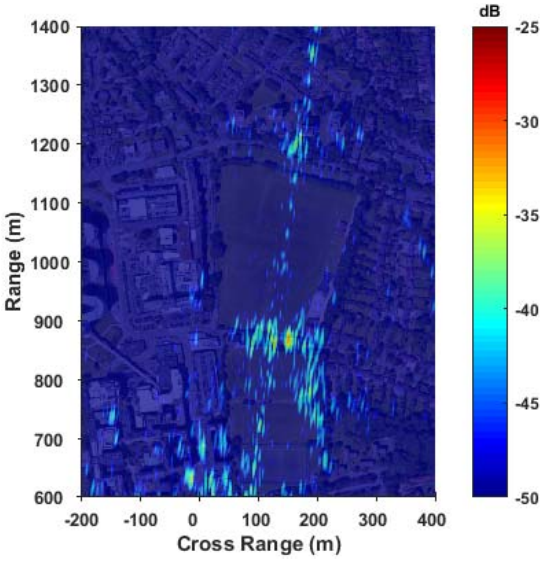


(a)

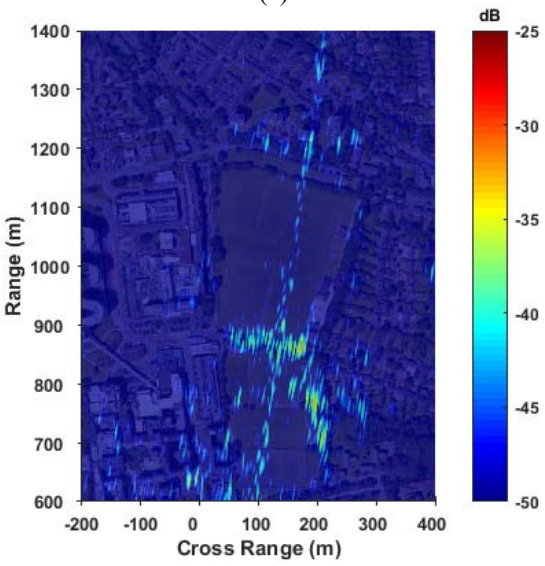


(b)

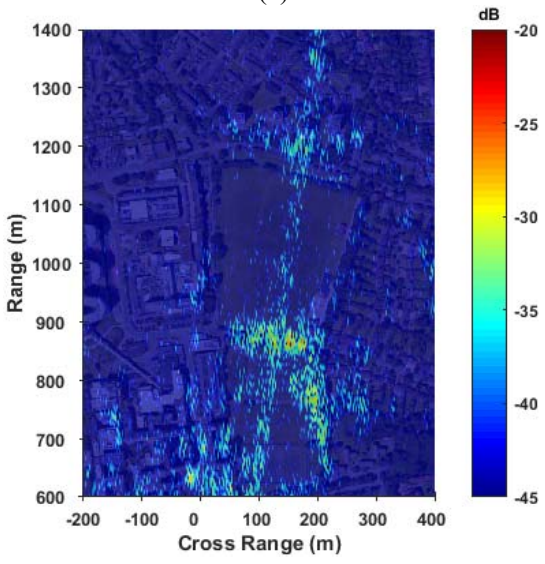


(c)

**Fig. 13 Experimental images (a) Bistatic image 1 (b) Bistatic image 2 and (c) Coherent multistatic image**

**Table 3 Spatial resolution comparison for Area A**

| Image | Cross-range (m) | Range (m) | Intensity (dB) |
|---|---|---|---|
| Bistatic 1 | 3.74 | 22.31 | -43.00 |
| Bistatic 2 | 3.61 | 15.42 | -42.26 |
| Coherent Multistatic | 1.27 | 8.69 | -35.80 |

**Table 4 Spatial resolution comparison for Area B**

| Image | Cross-range (m) | Range (m) | Intensity (dB) |
|---|---|---|---|
| Bistatic 1 | 5.03 | 21.02 | -32.28 |
| Bistatic 2 | 3.96 | 18.21 | -31.98 |
| Coherent Multistatic | 2.06 | 12.37 | -26.40 |

**Table 5 Spatial resolution comparison for Area C**

| Image | Cross-range (m) | Range (m) | Intensity (dB) |
|---|---|---|---|
| Bistatic 1 | 4.19 | 22.03 | -41.11 |
| Bistatic 2 | 3.95 | 18.29 | -43.42 |
| Coherent Multistatic | 1.62 | 9.36 | -35.97 |

(a)

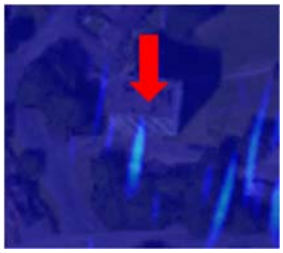

(b)

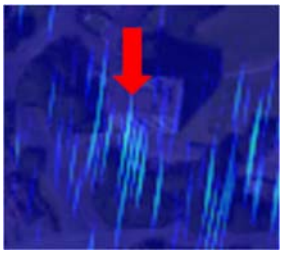

(c)

**Fig. 14 Enlargement of Area A from (a) Bistatic image 1 (b) Bistatic image 2 and (c) Coherent multistatic image**

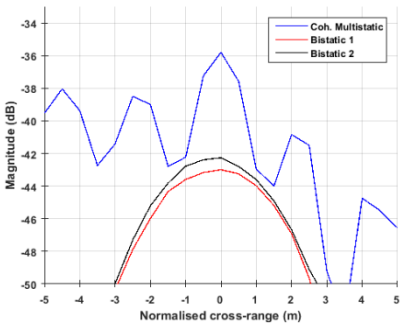


(a)

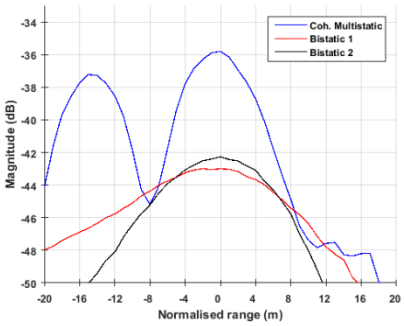


(b)

**Fig. 15 Comparison of cross-sectional profiles in (a) cross range and (b) range directions using PSFs extracted from Area A**

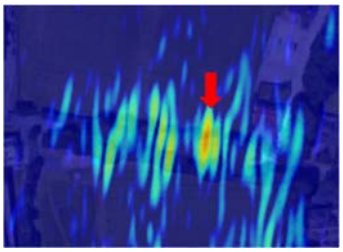

(a)

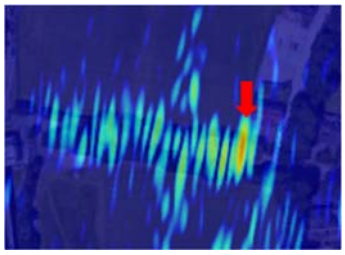

(b)

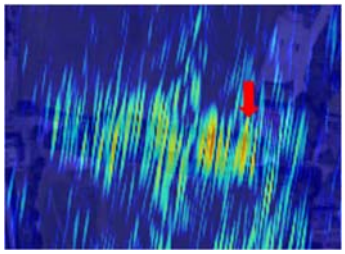

(c)

**Fig. 16 Enlargement of Area B from (a) Bistatic image 1 (b) Bistatic image 2 and (c) Coherent multistatic image**

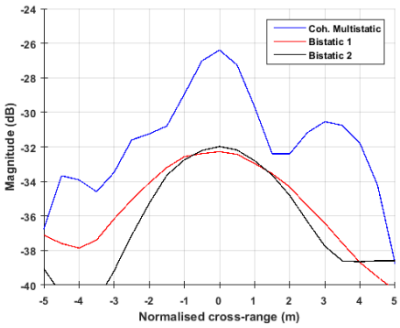


(a)

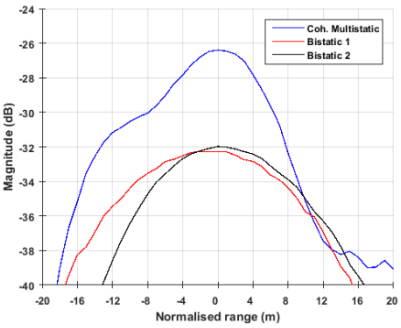


(b)

**Fig. 17 Comparison of cross-sectional profiles in (a) cross range and (b) range directions using PSFs extracted from Area B**

(a)

(b)

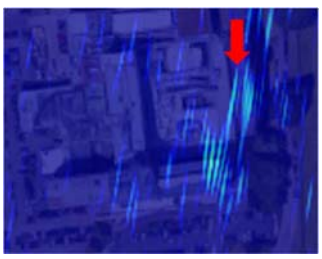

(c)

**Fig. 18 Enlargement of Area C from (a) Bistatic image 1 (b) Bistatic image 2 and (c) Coherent multistatic image**

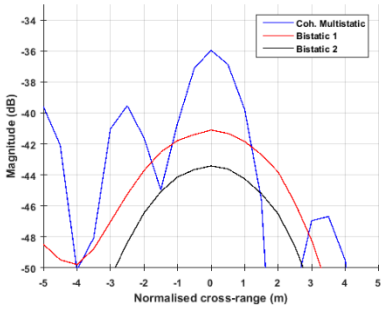


(a)

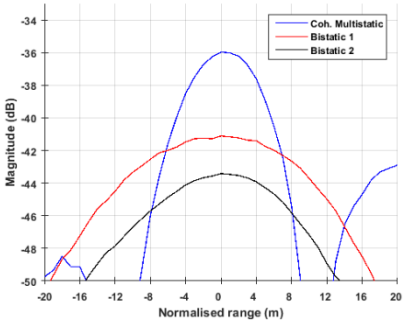


(b)

**Fig. 19 Comparison of cross-sectional profiles in (a) cross range and (b) range directions using PSFs extracted from Area C**

## 6. References


[1] Krysik, P., Kulpa, K., Samczynski, P., *et al.*: 'Moving target detection and imaging using GSM-based passive radar'. IET Int. Conf. Radar Syst., Glasgow, UK, October 2012, pp. 1-4

[2] Gutierrez Del Arroyo, J.R., Jackson J.A., 'WiMAX OFDM for passive SAR ground imaging', IEEE Trans. Aerosp. Electron. Syst., 2013, 49, (2), pp. 945-959

[3] Abiven, P., Lim, T.J., Pisane, J.: 'FM passive bistatic radar imaging of airplanes in a real configuration'. Int. Radar Conf., Lille, France, October 2014, pp. 1-6

[4] Gromek, D., Kulpa, K., Samczynski, P.: 'Experimental results of passive SAR imaging using DVB-T illuminators of opportunity', IEEE Geosci. Remote Sens. Lett., 2016, 13, (8), pp. 1124-1128

[5] Ulander, L.M.H., Frölind, P., Gustavsson, A., *et al.*: 'Airborne passive SAR imaging based on DVB-T signals'. in IEEE Geosci. Remote Sens. Symp., Fort Worth, TX, USA, July 2017, pp. 2408-2411

[6] Brisken, S., Moscadelli, M., Seidel, V., *et al.*: 'Passive radar imaging using DVB-S2'. IEEE Radar Conf., Seattle, WA, USA, May 2017, pp. 552-556

[7] Antoniou, M., Saini, R., Cherniakov, M.: 'Results of a space-surface bistatic SAR image formation algorithm', IEEE Trans. Geosci. Remote Sens., 2007, 45, (11), pp. 3359-3371

[8] Antoniou, M., Cherniakov, M., Hu, C.: 'Space-surface bistatic SAR image formation algorithms', IEEE Trans. Geosci. Remote Sens., 2009, 47, (6), pp. 1827-1843

[9] Antoniou, M., Cherniakov, M.: 'GNSS-based bistatic SAR: a signal processing view', EURASIP J. Adv. Signal Process., 2013, 2013, (1), pp. 1-16

[10] Cherniakov, M., Saini, R. Zuo, Z., *et al.*: 'Space-surface bistatic synthetic aperture radar with global navigation satellite system transmitter of opportunity-experimental results', IET Radar Sonar Navig., 2007, 1, (6), pp. 447-458

[11] Cherniakov, M., Zeng, T.: "Space-surface bistatic SAR," in M. Cherniakov, M. (Ed.): 'Bistatic Radar: emerging technology' (John Wiley & Sons, Chichester, 2008, 1st edn.), ch. 6, pp. 215-246

[12] Antoniou, M., Zeng, Z., Feifeng, L., *et al.*: 'Experimental demonstration of passive BSAR imaging using navigation satellites and a fixed receiver', IEEE Geosci. Remote Sens. Lett., 2012, 9, (3), pp. 477-481

[13] Liu, F. Antoniou, M., Zeng, Z., *et al.*: 'Point spread function analysis for BSAR with GNSS transmitters and long dwell times: theory and experimental confirmation', IEEE Geosci. Remote Sens. Lett., 2013, 10, (4), pp. 781-785

[14] Antoniou, M., Hong, Z., Zeng Z., *et al.*: "Passive bistatic synthetic aperture radar imaging with Galileo transmitters and a moving receiver: experimental demonstration', IET Radar Sonar Navig., 2013, 7, (9), pp. 985-993

[15] Antoniou, M., Cherniakov, M.: 'GNSS-based passive radar', in Klemm, R., Nickel, U., Gierull, C. (Eds.): 'Novel Radar Techniques and Applications Volume 1: Real Aperture Array Radar, Imaging Radar, and Passive and Multistatic Radar' (SciTech Publishing, London, 2017, 1st edn.), ch. 16, pp. 719-766

[16] Ma, H., Antoniou, M., Cherniakov, M.: 'Passive GNSS-based SAR resolution improvement using joint Galileo E5 signals', IEEE Geosci. Remote Sens. Lett., 2015, 12, (8), pp. 1640-1644

[17] Nithirochananont, U., Antoniou, M., Cherniakov, M.: 'Passive multi-static SAR – experimental results', IET Radar Sonar Navig., 2019, 13, (2), pp. 222-228

[18] Santi, F., Antonio, M., Pastina, D.: 'Point spread function analysis for GNSS-based multistatic SAR', IEEE Geosci. Remote Sens. Lett., 2015, 12, (2), pp. 304-308

[19] F. Santi, F., Bucciarelli, M., Pastina, D., *et al.*: 'Spatial resolution improvement in GNSS-based SAR using multistatic acquisitions and feature extraction', IEEE Trans. Geosci. Remote Sens., 2016, 54, (10), pp. 6217-6231

[20] Prati, C., Rocca, F.: 'Improving slant-range resolution with multiple SAR surveys', IEEE Trans. Aerosp. Electron. Syst., 1993, 29, (1), pp. 135-143

[21] F. Gatelli, F., Monti Guamieri, A., Parizzi, F., *et al.*: 'The wavenumber shift in SAR interferometry',

IEEE Trans. Geosci. Remote Sens., 1994, 32, (4), pp. 855-865

[22] Guillaso, S., Reigber, A., Ferro-Famil, L., *et al.*: 'Range resolution improvement of airborne SAR images', IEEE Geosci. Remote Sens. Lett., 2006, 3, (1), pp. 135-139

[23] G. Fornaro, G., Pascazio, V., Schirinzi, G., *et al.*: 'Multi-pass ENVISAT-ASAR data processing for improved resolution imaging'. IEEE Geosci. Remote Sens. Symp., Denver, CO, USA, August 2006, pp. 2553-2556

[24] Rennich, P.K., Casciato, M.D., Chan, A.M., *et al.*: "Coherent multistatic SAR collections and target phenomenology'. European Radar Conf., Amsterdam, Netherlands, October 2008, pp. 152-155

[25] Yang, C., Zeng, T., Ding Z.: 'A high resolution multiple-receiver SS-BSAR system'. IET Int. Radar Conf., Guilin, China, April 2009, pp. 1-5

[26] Ginolhac, G., Schmitt, F., Daout, F., *et al.*: 'Multifrequency and multistatic inverse synthetic aperture radar, with application to FM passive radar', EURASIP J. Adv. Signal Process., 2009, 2010, (1), pp. 1-13

[27] Van Dorp, P., Otten, M.P.G., Verzeilberg J.M.M.: 'Coherent multistatic ISAR imaging'. IET Int. Conf. Radar Syst., Glasgow, UK, October 2012, pp. 1-6

[28] Garry, J.L., Baker, C.J., Smith, G.E., *et al.*: 'Investigations toward multistatic passive radar imaging'. IEEE Radar Conf., Cincinnati, OH, USA, May 2014, pp. 607-612

[29] Samczynski, P., Kulpa, K., Baczyk, M.K., *et al.*: 'SAR/ISAR imaging in passive radars'. IEEE Radar Conf., Philadelphia, PA, USA, May 2016, pp. 1-6

[30] Tebaldini, S., Rocca, F.: 'Multistatic wavenumber tessellation: Ideas for high resolution P-band SAR missions'. IEEE Geosci. Remote Sens. Symp., Fort Worth, TX, USA, 2017, pp. 2412-2415

[31] Jakowatz, C.V.J., Wahl, D.E., Eichel, P.H., *et al.*: 'Spotlight-mode synthetic aperture radar: a signal processing approach' (Kluwer Academic, London, 1996, 1st edn.)

[32] Ender J.H.G.: 'The meaning of k-space for classical and advanced SAR-techniques'. Int. Symp. Phys. Signal Image Process., Marseille, France, January 2001, pp. 23-38

[33] Zeng, T., Dongyang, A., Cheng, H., *et al.*: 'Comparison between monostatic and bistatic SAR image based on spatial spectrum analysis'. IET Int. Radar Conf., Hangzhou, China, October 2015, pp. 1-6

[34] Mao, X., Zhang, Y.D., Amin, M.G.: 'Low-complexity sparse reconstruction for high-resolution multi-static passive SAR imaging', EURASIP J. Adv. Signal Process., 2014, 2014, (1), pp. 1-12

[35] Ma, H., Cherniakov, M., Pany, T., *et al.*: 'Galileo-based bistatic SAR imaging using joint E5 signals: experimental proof-of-concept'. Int. Conf. Radar Syst., Belfast, UK, October 2017, pp. 1-5

[36] Zhang, Q., Antoniou, M., Chang, W., *et al.*: 'Spatial decorrelation in GNSS-based SAR coherent change detection', IEEE Trans. Geosci. Remote Sens., 2015, 53, (1), pp. 219-228

[37] Salzman, J., Akamine, D., Lefevre, R., *et al.*: 'Interrupted synthetic aperture radar (SAR)', IEEE Aerosp. Electron. Syst. Mag., 2002, 17, (5), pp. 33-39

[38] Nithirochananont, U., Antoniou, M., Cherniakov, M.: 'Passive coherent multistatic SAR: experimental results with a point-like target'. Int. Radar Symp., Ulm, Germany, June 2019, pp. 1-6

[39] Larsson, E.G., Stoica, P., Li, J.: 'Amplitude spectrum estimation for two-dimensional gapped data', IEEE Trans. Signal Process.,2002, 50, (6), pp. 1343-1354

[40] Vu, D., Xu, L., Xue, M., *et al.*: "Nonparametric missing sample spectral analysis and its applications to interrupted SAR', IEEE J. Sel. Topics Signal Process, 2012, 6, (1), pp. 1-14

[41] Griffiths, H.D., Baker, C.J.: 'Passive coherent location radar systems. part 1: performance prediction', IEE Radar Sonar Navig., 2005, 152, (3), pp. 153-159

[42] Garry, J.L. Baker, C.J., Smith, G.E.: 'Evaluation of direct signal suppression for passive radar', IEEE Trans. Geosci. Remote Sens, 2017, 55, (7), pp. 3786-3799

[43] Saini, R., Cherniakov, M., Lenive, V.: 'Direct path interference suppression in bistatic system: DTV based radar'. IEEE Int. Conf. Radar, Adelaide, Australia, September 2003, pp. 309-314

[44] Tao, R., Wu, H.Z., Shan, T.: 'Direct-path suppression by spatial filtering in digital television terrestrial broadcasting-based passive radar', IET Radar Sonar Navig., 2010, 4, (6), pp. 791-805